ACS APPLIED MATERIALS & INTERFACES

Research Article

www.acsami.org

Mesoporous Hollow Sphere Titanium Dioxide Photocatalysts through Hydrothermal Silica Etching

Tim Leshuk,[†,‡] Stuart Linley,[†,‡] George Baxter,[‡] and Frank Gu*[,‡,§]

[‡]Department of Chemical Engineering, [§]Waterloo Institute for Nanotechnology, University of Waterloo, Waterloo, Ontario, Canada.

Supporting Information

ABSTRACT: Robust, monodisperse, mesoporous titanium dioxide (TiO_2) submicrometer hollow spheres were synthesized through a single step hydrothermal silica etching reaction under mild conditions. Efficient silica (SiO_2) removal was achieved without the use of toxic reagents, and a unique controllable silica redeposition mechanism was identified, imparting the hollow spheres with excellent structural integrity. The parameters of the hydrothermal reaction affecting the etching process, including pH, temperature, and silica concentration, were systematically investigated and optimized for the production of silica-templated hollow structures. The resulting processing conditions yielded TiO_2 hollow spheres with a surface area of ~300 m^2 g^{-1} and anatase phase crystallization, which exhibited high adsorption capacity for methylene blue dye and good photocatalytic activity without requiring high-temperature calcination.

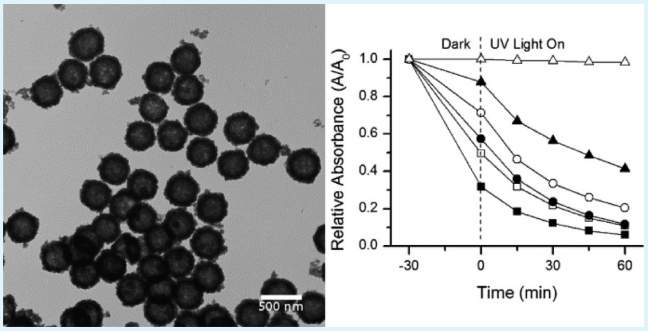

KEYWORDS: *green chemistry, titanium dioxide, photocatalysis, hollow, one pot, hydrothermal*

1. INTRODUCTION

Titanium dioxide is an important material in many areas of science and engineering, and is a topic of much ongoing research and development.[1−3] Its many applications range from use in consumer products such as sunscreens, paints, toothpastes and food, to higher technologies such as photovoltaics and photocatalysis.[4−6] Due to its chemical inertness and nontoxicity, high photocatalytic efficiency, and ability to successfully degrade a large number of environmental pollutants, TiO_2 photocatalysis has been recognized as one of the most promising advanced water treatment methods.[6−8] Much of the recent research into TiO_2 materials for photocatalysis focused on developing high-surface-area nanomaterials with improved light utilization, for example nanospheres, nanotubes, and mesoporous structures, in order to elicit improved photocatalytic performance.[9−12] These nanostructures typically have much higher specific surface areas than bulk TiO_2, allowing for shorter charge carrier diffusion path lengths and facilitating increased electrochemical reactions at the aqueous interface. Among these new morphologies, hollow spheres have garnered much attention because they offer several advantages over their nonhollow counterparts such as higher surface area, lower effective particle density, and better light harvesting, which all contribute to increasing the efficacy of TiO_2 as a photocatalyst.[13−20] Recently, special mechanisms of light trapping unique to the hollow sphere morphology, such as multiple internal reflections and whispering gallery mode resonance, have been of particular research interest, where enhanced light collection is important for a variety of optoelectronic applications.[21−24]

Current strategies for synthesizing hollow structures mostly involve using a "hard templating" method whereby TiO_2 is deposited on a solid core which is later removed, leaving only a TiO_2 shell. The most common template materials for hard templating are monodispersed microspheres, such as polymeric, latex or Stöber silica particles.[15,25,26] Although hard templating methods offer advantages in providing fine control of the size distribution and dimensions of the hollow structures, the removal of template cores requires the use of toxic solvents or dangerous chemical etchants. For example, SiO_2 is often etched using hydrofluoric acid, which can be difficult to handle and makes the synthesis process less convenient or environmentally appealing.[16,23,27,28] High-surface-area mesoporous shells can also be difficult to prepare with templated hollow sphere particles.

In contrast to the hard templating processes described above, the hydrothermal technique is less toxic because of the use of water as the primary solvent, although it is often more difficult to control elaborate or templated structures in the hydrothermal system because of the extremely high reactivity of the aqueous milieu above the boiling point of water.[29,30] Hydrothermal processing has proven especially useful to introduce disordered mesophases to TiO_2 without the need for templating surfactants, improve the materials' hydrophilicity due to an increase of surface hydroxyl groups, and allow access

Received: August 17, 2012
Accepted: October 30, 2012
Published: October 30, 2012

to photocatalytically active crystalline phases at much lower temperatures than is required for air calcination.[31,32]

Herein we report a one-pot synthesis method for producing size-controlled mesoporous hollow TiO_2 spheres through combining the advantages of both hard templating and hydrothermal processing. The advantage of this synthesis method is that in a single aqueous reaction step, the core templates are selectively removed, and a mesoporous, photocatalytically active crystalline phase of TiO_2 is simultaneously formed within the spherical shell at mild temperature without the need for calcination, all while preserving the advantages of the template approach, namely, having good synthesis control over core and shell dimensions, and high monodispersity (Scheme 1). The resulting hollow particles possess exceptionally high surface areas and exhibit superior surface adsorption capacity and photocatalytic activity compared with the corresponding nonhollow spheres and calcined hollow spheres. We identified the reaction parameters affecting the behavior of silica templates under hydrothermal conditions, and present optimized conditions for achieving efficient and selective silica etching. Furthermore, this process allows for the controllable redeposition of silica in the hollow shell during the hydrothermal treatment, which behaves as a binder and provides excellent structural integrity to the hollow spheres.

Scheme 1. Conceptual Overview of the Hydrothermal Synthesis Method Used in This Study

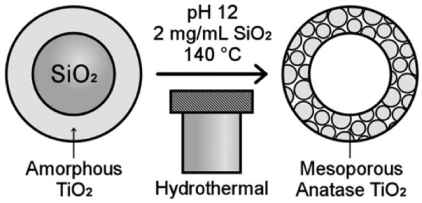

2. RESULTS AND DISCUSSION

The synthesis of the hollow spheres can be summarized as follows: first, precursor particles to the hollow spheres, amorphous TiO_2-coated SiO_2 core–shell (SiO_2@TiO_2) spheres, are prepared through sol–gel colloidal chemistry, followed by a hydrothermal treatment to remove the SiO_2 core template and simultaneously crystallize and porosify the TiO_2 shell (Scheme 1). The reaction parameters controlling the hydrothermal etching process, including reaction temperature, reaction time, silica concentration, and pH, were serially optimized for the efficient formation of resilient hollow spheres.

2.1. Synthesis of SiO_2@TiO_2 Precursor Particles. The sol–gel method established by Stöber et al. was used to produce the SiO_2 template particles (~350 nm mean diameter).[33] The Stöber method is especially useful for the production of template materials for hollow particles as the size of the silica particles can be easily controlled with good precision in the submicrometer size domain, and excellent monodispersity in particle size distributions.[33,34] A layer of amorphous TiO_2 was subsequently deposited on the surface of these SiO_2 core particles by a single-step colloidal sol–gel reaction.[35] TEM characterization confirmed the presence of TiO_2 on the particle surface by the appearance of a rough coating (Figure 1) and an overall particle size increase to approximately 450 nm, indicating a ~50 nm thick shell had been deposited (Figure 1). It can also be observed that the monodispersity of the particles was preserved through the coating process (<5% standard deviation in mean diameter, n = 193), without interparticle aggregation. Although other studies using similar TiO_2 deposition chemistry were required to perform multiple sequential coating reactions to build up the thickness of the amorphous TiO_2 shell,[35,36] in this work, we have tuned the concentration of silica core particles to achieve a substantially thick shell in a single step, increasing the simplicity and convenience of preparing the precursor particles for hollow sphere formation.

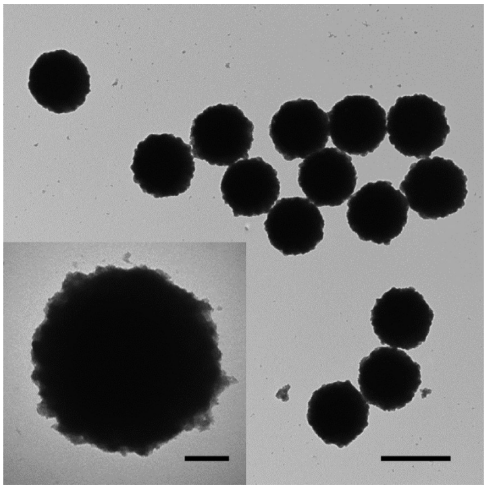

Figure 1. TEM images of the SiO_2@TiO_2 precursor particles (SiO_2 spheres coated with amorphous TiO_2). Scale bar is 500 nm, inset scale bar is 100 nm.

2.2. Hollow Sphere Synthesis. *2.2.1. pH Variation.* The first hydrothermal parameter optimized was the pH of the particle suspension. It is well established that alkaline solutions enhance the dissolution of silica through base hydrolysis, the reverse reaction of the condensation used to produce the silica cores.[37] The SiO_2@TiO_2 particles were dispersed into water such that the final silica concentration was 3 mg mL^{-1}, and NaOH solution was added to attain pH values of 7, 10, 12, and 14. These particle suspensions were then sealed in pressure vessels and subjected to hydrothermal treatment at 180 °C for 12 h. The initial temperature for the hydrothermal reaction was chosen to be 180 °C, as previous studies indicated that this temperature resulted in optimal TiO_2 photocatalytic activity.[32]

TEM images of the particles after the hydrothermal treatment are presented in Figure 2. As shown in Figure 2a, at pH 7 the particles remained relatively unchanged compared to the precursor SiO_2@TiO_2 particles (Figure 1) with respect to hollowness, and the only observable difference between these samples was the apparent coarsening of the TiO_2 shell as a result of the hydrothermal treatment. During hydrothermal treatment, amorphous TiO_2 is known to experience a phase change to anatase via a dissolution and reprecipitation process, wherein transiently dissolved titanate species rapidly nucleate to form nanocrystalline structures due to the high reactivity of the hydrothermal system.[11,38] That is, hydrothermal water attacks the amorphous TiO_2 from the solid–liquid interface, causing condensation of the amorphous structure to form aggregated nanocrystals. This process thusintroduces a disordered mesoporosity to the TiO_2 through an Ostwald ripening mechanism,[11,32] which allows the hydrothermal water to penetrate deeper into the shell and react with residual amorphous TiO_2.[39] This porosification process accounts for

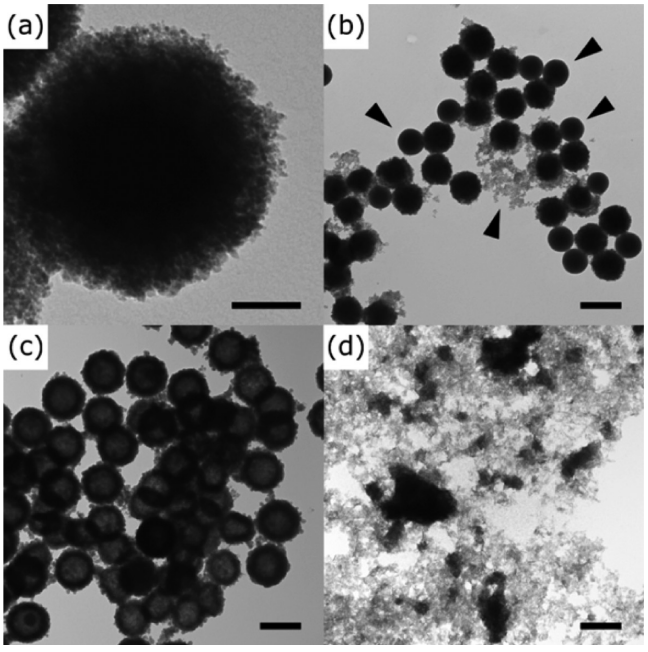

Figure 2. TEM images of the particles after hydrothermal treatment (3 mg mL^{-1} SiO_2, 180 °C, 12 h) at different pH conditions: (a) pH 7, (b) pH 10, (c) pH 12, and (d) pH 14. Arrows indicate uncoated spheres and free TiO_2. Scale bars are 100 nm for a, and 500 nm for b–d.

the observed coarse granular structure of the TiO_2 shell. No hollow spheres were formed at pH 10 (Figure 2b), although a number of uncoated and partially coated SiO_2 spheres were observed, along with substantial free TiO_2 dissociated from the silica cores. We postulate that this stripping of the TiO_2 shell, as compared to the intact core–shell structure of the pH 7 treatment, may have been due to the partial dissolution of the outside of the SiO_2 cores.

The expectation of base enhanced silica dissolution was demonstrated in the pH 12 hydrothermal experiment, which yielded hollow sphere structures, easily discernible by contrasting the darker shell of the particles with their lighter and empty interiors (Figure 2c). The overall diameter of the hollow spheres was ~500 nm, with a shell thickness of ~75 nm, indicating a slight swelling of the particles from the hydrothermal processing. The presence of a small population of rattle particles, i.e., hollow spheres encapsulating a smaller residual SiO_2 particle, suggests that the hydrothermal silica etching process is initiated from the outer surface of the SiO_2 core and proceeds inward until the core has been completely dissolved. The silicate monomers diffuse from the interior of the particle through the porous TiO_2 shell, and possibly redeposit as silica on the outer surface of the hollow spheres as the bulk concentration of silicate exceeds saturation. Silica redeposition could explain why the pH 12 spheres did not disintegrate as the shells in the pH 10 sample did (Figure 2b), where the total amount of dissolved and subsequently redeposited silica would have been insufficient to preserve the shell structure throughout the entire hydrothermal treatment.

At pH 14 the silica cores were entirely dissolved in a similar manner as in the pH 12 experiment, however no semblance of hollow TiO_2 shells survived the hydrothermal process either (Figure 2d). It is possible that at higher pH, the solubility of the amorphous TiO_2 was increased in a similar fashion as is the solubility of silica, and that the dissolution and recrystallization process whereby the nanocrystalline TiO_2 shells were purported to form became primarily a dissolution process without any reprecipitation. Thus pH 12 appeared to be optimal for the formation of hollow structures under the hydrothermal conditions tested.

2.2.2. Concentration Variation. We next analyzed the effect of silica concentration on the hydrothermal etching process, and optimized this concentration for the efficient formation of hollow spheres. The experiments were performed at pH 12 and hydrothermally treated at 180 °C for 12 h as previously, loading different amounts of SiO_2@TiO_2 precursor particles for the different test conditions, varying the total SiO_2 concentration from 0.5 − 3 mg mL^{-1}. The highest concentration of silica tested, 3 mg mL^{-1}, demonstrated incomplete silica dissolution, with a substantial number of residual rattle spheres remaining (Figure 3a). On decreasing the total SiO_2 concentration to 2 mg mL^{-1}, the population of rattle particles was substantially reduced, while the hollow structure of the particles remained intact, indicating that a solubility limit may have been exceeded in the 3 mg mL^{-1} SiO_2 reaction, and that 2 mg mL^{-1} SiO_2 was the optimal concentration for stable hollow sphere formation.

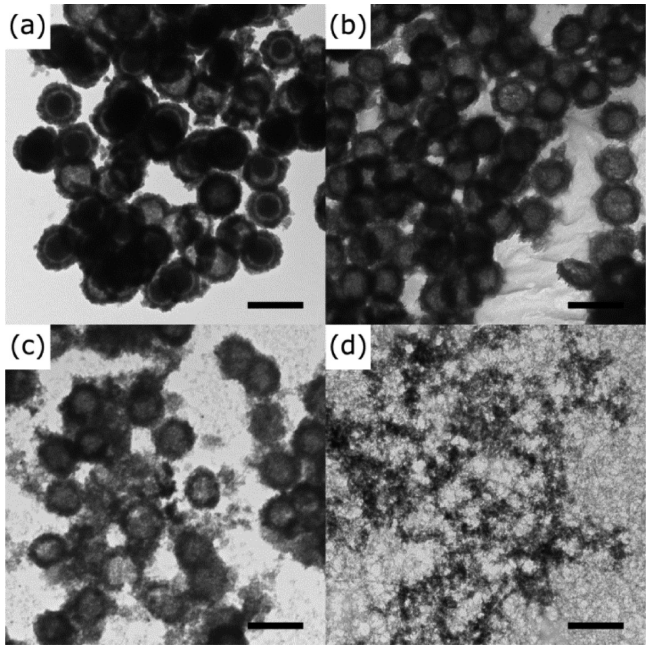

Figure 3. TEM images of the particles after hydrothermal treatment (pH 12, 180 °C, 12 h) at different SiO_2 concentrations: (a) 3, (b) 2, (c) 1, and (d) 0.5 mg mL^{-1}. Scale bars are 500 nm.

Further decreasing the total SiO_2 concentration to 1 and 0.5 mg mL^{-1} adversely affected the structural integrity of the remaining TiO_2, as seen in Figure 3c, d. Indeed, only a fine sol of TiO_2 nanoparticles was formed in the 0.5 mg mL^{-1} reaction, similar to TiO_2 hydrothermal syntheses reported in the literature.[31,32,40]

One explanation for the destruction of the spherical structures at lower concentrations is that the relative amount of soluble TiO_2 may have been effectively increased, compromising the shell integrity. An alternative explanation is that silica redeposition is in fact essential to maintain the hollow sphere morphology of the TiO_2 shell in the intense hydrothermal milieu, in that the redeposited silica may act as a binder material to cross-link the TiO_2 nanocrystals in the shell

dx.doi.org/10.1021/am3016922 | ACS Appl. Mater. Interfaces 2012, 4, 6062–6070

and prevent their dispersion due to thermal motion throughout the course of the hydrothermal treatment. Such a scenario would account for the stable hollow spheres formed at higher silica concentrations, and the disintegrating spheres formed at lower concentrations, where insufficient silica redeposited to preserve the hollow sphere morphology. Poor silica redeposition could also explain the previous pH 14 disintegration result (Figure 2d), as less silica would be expected to redeposit in the shell structure due to the enhanced solubility of silica in strong base. Indeed, some samples showed clear signs of redeposited silica on TEM (Figure 2a, and the Supporting Information, Figure 1).

As a further step of optimization, we investigated the effect of total hydrothermal reaction time at these conditions. It would be preferable to minimize the hydrothermal treatment time, as not only would an excessively long heating time increase the cost of the processing, but it would allow for continuous Ostwald ripening of the TiO_2 nanocrystals in the shell,[32] which could undesirably reduce the specific surface area of the hollow spheres. At 2 mg mL^{-1} SiO_2, pH 12, and 180 °C, 1.5 h of hydrothermal treatment produced a higher number of rattle particles (SI Figure 2a), while the number of rattles was substantially reduced in a sample treated for 6 h (SI Figure 2b), with predominate hollow sphere particles remaining as in the 12 h treatment. Thus 6 h at these hydrothermal conditions was deemed to be sufficient time for the system to reach equilibrium in terms of dissolved silica.

2.2.3. Temperature Variation. We proceeded to study the effect of reaction temperature, a critical variable in hydrothermal TiO_2 synthesis,[32] on the formation of the hollow spheres. Using optimal reaction conditions from the previous studies (pH 12, 2 mg mL^{-1} SiO_2, 6 h reaction time), three hydrothermal reactions were performed at different temperatures, 140, 180, and 220 °C. The effect of this temperature variation on the microstructure of the hollow spheres is shown in Figure 4; the differences between the 140 and 220 °C reactions are especially striking. Although the particles formed at 140 °C appear to be ideal mesoporous hollow spheres of nearly perfect spherical geometry (Figure 4a), the spheres prepared at 220 °C are partially degraded, where some of the hollow spheres appear to have collapsed into mesoporous aggregates or disintegrated (Figure 4b). The poorer structural integrity of the 220 °C hollow spheres may be due to increased thermal diffusion forces acting on the TiO_2 nanocrystals in the shell structure at higher temperatures, as well as the increased solubility of silica at higher hydrothermal temperatures.[41]

The nanocrystals comprising the shells of the 140 °C spheres also appear to be much finer than those in the 220 °C sample, which are notably larger and coarser (Figure 4c, d, and the Supporting Information, Figure 3). This result can be explained by the increase of the solubility of TiO_2 with hydrothermal temperature, facilitating accelerated Ostwald ripening of the nanocrystals within the particle shells.[32] A larger nanocrystal size distribution would be expected to decrease the surface area of the hollow spheres as a whole, therefore we performed N_2 adsorption to characterize the specific surface area of the hollow spheres prepared at the different temperatures, the results of which are presented in Table 1 (N_2 adsorption data is in Table S1 in the Supporting Information). The specific surface area of the 140 °C hollow spheres, at ~300 m^2 g^{-1}, is exceptional for mesoporous TiO_2 materials, and even the hollow spheres prepared at 180 and 220 °C significantly exceed previously reported mesoporous TiO_2 hollow spheres in terms of surface

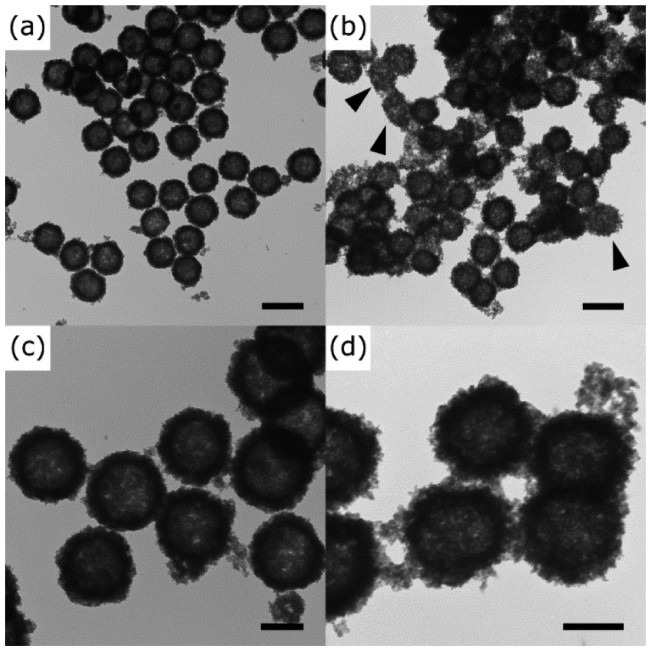

Figure 4. TEM images of the particles after hydrothermal treatment (pH 12, 2 mg mL^{-1} SiO_2, 6 h) at different reaction temperatures: (a, c) 140 °C, (b, d) 220 °C. Arrows indicate spheres with poor structural integrity. Scale bars are 500 nm for a and b, and 200 nm for c and d.

area.[10,21,42] For example, recently reported mesoporous TiO_2 hollow spheres prepared from carbon microsphere templates exhibited a specific surface area of 74 m^2 g^{-1}, with less uniform sphere morphology, and greater intersphere aggregation.[21] The high surface area of the hollow spheres reported herein is attributed to the formed TiO_2 nanocrystallites within the shell (as discussed in Section 2.2.1 above), where the 140 °C spheres with the highest surface area possess the finer nanocrystals.[10,39] Thus one of the objectives for our current work, to combine the advantages offered by hydrothermal processing with a hard templating approach to form hollow spheres, is validated by these surface areas.

We also performed XRD to investigate the crystallinity of the prepared samples. The XRD patterns obtained for all the hollow sphere samples could be indexed to anatase phase TiO_2 (Figure 5a). Only incipient crystallinity was present in the 140 °C sample, whereas the 220 °C sample was substantially better crystallized. Similarly, the mean crystal size detected by XRD was only 3.5 nm for the 140 °C sample, increasing to 5.2 nm for the 240 °C sample (Table 1). Because of the increased solubility of TiO_2 at higher temperature, transiently dissolved titanate species can more readily rearrange to form more thermodynamically favorable crystal structures, whereas the crystallization process may be prematurely arrested in the lower temperature samples due to insufficient energy for the topotactic transformation. Thus there exists a trade-off between specific surface area and crystallinity when selecting the hydrothermal temperature to use in hollow sphere formation, although the silica cores were equivalently completely removed at all three reaction temperatures.

We next determined the relation between temperature and pH in the etching process, and whether hydrothermal temperatures were necessary to form TiO_2 hollow spheres. We thus attempted to prepare a hollow sphere sample at room temperature (pH 12, 2 mg mL^{-1} SiO_2). It would appear that

dx.doi.org/10.1021/am3016922 | ACS Appl. Mater. Interfaces 2012, 4, 6062−6070

Table 1. BET Surface Areas and Average Crystallite Sizes for Hollow Spheres Prepared at Different Hydrothermal Temperatures.[a]

hydrothermal temperature (°C)	140	180	220	140[c]
BET surface area [m^2 g^{-1}]	298.0 ± 1.0	223.7 ± 1.4	196.6 ± 1.2	162.9 ± 0.5
average crystallite size (nm)[b]	3.5	5.0	5.2	4.0

[a]Prepared at pH 12, 2 mg mL^{-1} SiO_2, 6 h treatment time. [b]Calculated from the (101) XRD peak using the Scherrer equation. [c]Sample subsequently calcined at 500 °C, and then base etched to remove residual silica.

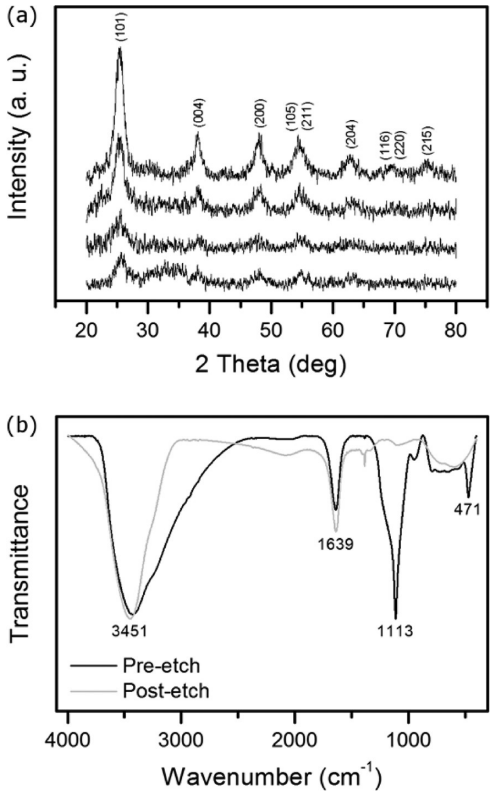

Figure 5. (a) XRD patterns for samples treated under various thermal processing conditions. Patterns correspond to (from top to bottom): hollow spheres hydrothermally synthesized at 220, 180, and 140 °C, and hollow spheres hydrothermally synthesized at 140 °C then calcined at 500 °C and base etched. (b) FTIR spectra of hollow spheres hydrothermally synthesized at 140 °C, showing the presence and removal of residual silica before and after calcination and base etching. The black line corresponds to the hollow spheres before calcination, whereas the gray line corresponds to the sample after calcination and base etching.

apart from crystallizing the mesoporous hollow spheres, the higher temperature also significantly accelerates the etching process, as only rattle particles were produced from the room temperature reaction after 5 days (see the Supporting Information Figure 4), and hollow spheres could not be formed at room temperature with equivalent total silica concentrations as were used in the hydrothermal reactions.

It should also be noted that this hydrothermal silica etching process does not appear to be dependent on the SiO_2 core size. Smaller SiO_2 spheres (~150 nm mean diameter) were synthesized and coated with an amorphous TiO_2 shell as previously (see the Supporting Information, Figure 5a), and were then subjected to the same hydrothermal treatment conditions as the larger SiO_2@TiO_2 particles had been (i.e., pH 12, 2 mg mL^{-1} SiO_2, 140 °C, 6 h). It was thus quite simple to obtain smaller mesoporous hollow spheres (see the Supporting Information, Figure 5b). This straightforward size control is one of the primary advantages of using Stöber SiO_2 spheres as a template material, and these results also demonstrate the general applicability of the optimized SiO_2 etching conditions described above.

2.3. Residual Silica and Calcination. We next determined the role of the residual silica (see the Supporting Information, Figure 2) hypothesized to redeposit in the shell during or after the hydrothermal etching process and to act as a binder material maintaining the hollow shell structure. We intended to test this theory by removing the residual silica through a second etching step with strong base, and then observing whether the structural integrity of the hollow spheres could be maintained in its absence. However, our initial experiments showed that the hollow spheres could not survive such a treatment with strong base (Figure 2d), although calcined TiO_2 has been shown to be sufficiently resilient to etching by a strong base in previous literature reports.[36,42]

Therefore, the three hollow sphere samples from the hydrothermal temperature study (treated at 140, 180, and 220 °C) were subsequently calcined at 500 °C in air for 2 h,

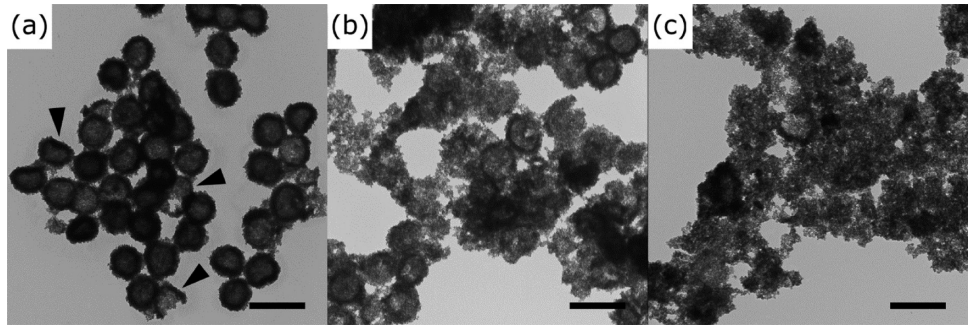

Figure 6. TEM images of particles after calcination at 500 °C for 2 h and subsequent etching with 0.5 m NaOH for 24 h at 50 °C, hydrothermally synthesized at different reaction temperatures: (a) 140, (b) 180, and (c) 220 °C. Arrows indicate broken and deformed spheres. Scale bars are 500 nm.

and then etched with 0.5 M NaOH for 24 h at 50 °C to remove residual silica. The resultant samples are shown in Figure 6.

Only the 140 °C sample largely maintained its structure through calcination and base etching (also confirmed with SEM, see the Supporting Information, Figure 6). The survival of these spheres may have been due to either incomplete residual silica removal, or sintering of the TiO_2 nanocrystals in the shell during calcination, obviating the need for any type of binding material to maintain structural integrity. Indeed, smaller nanocrystals, as were present in the 140 °C spheres relative to those in the spheres formed at higher hydrothermal temperatures, are especially susceptible to melting and sintering.[43,44] The BET surface area of the 140 °C hollow spheres was measured to decrease by 45% to 162.9 $m^2\ g^{-1}$ following calcination (Table 1), wherein loss of surface area is a typical result of particle sintering.[9,29] EDX confirmed the presence of a Si content of 15.7 at % in the 140 °C hollow spheres prior to calcination and base etching (see the Supporting Information, Table 1), and FTIR identified the identity of this residual Si to be in the form silica, revealed by the presence of a strong absorption peak at 1113 cm^{-1}, characteristic of Si−O−Si bonds (Figure 5b).[45,46] This peak disappeared from the FTIR spectrum following calcination and base etching of this sample (Figure 5b), whereas EDX showed an 82% drop in Si content of the spheres to only 2.8 at % (see the Supporting Information, Table 1), indicating that the residual silica was indeed successfully removed by the strong base etch, and that sintering of the 140 °C hollow shells during calcination is the more probable explanation for their resistance to breakage following the base etch.

Intriguingly, the crystallinity of the surviving calcined hollow spheres was apparently not increased as a result of calcination, with negligible difference between the pre- and postcalcination XRD patterns (Figure 5a). Thus it would seem that the hollow spheres hydrothermally treated at 140 °C were already fully crystalline, with minimal crystal grain growth during calcination (Table 1). It is possible that the residual silica present in the hollow sphere shells may have inhibited the TiO_2 crystal grain growth that typically occurs during calcination at high temperature, as has been observed in recent publications.[36,47,48] Thus the high energy calcination step that is typically needed to crystallize amorphous TiO_2 into photocatalytically active phases[2,18,32,49] is not required for these hollow spheres, rendering the synthesis process more environmentally friendly and cost-effective. However, if calcination is necessary, it is possible that the residual silica may act as an impurity phase during the crystallization of the TiO_2 shell, and to reduce its concentration further, a more mild etching process may be attempted prior to calcination, such as room-temperature HF etching.

2.4. Photocatalysis. Photocatalysis is one of the most heavily researched applications of TiO_2 nanomaterials, and as the prepared mesoporous hollow spheres exhibited exceptional surface areas and good crystallinity, both highly desirable properties in photocatalysis, we thought they showed great promise for photocatalysis. Furthermore, we were interested in exploring the variation of the functional properties of the hollow spheres with respect to their synthesis conditions. The results of these photocatalytic tests are shown in Figure 7.

The hydrothermally treated hollow spheres all show excellent photocatalytic activity, almost completely decolouring the dye solution within 1 h of UV light exposure (Figure 7). Perhaps one of the most initially prominent features of the photocatalytic degradation curves is the strong dark adsorption of the hollow spheres in the 30 min before the test began, up to 42 mg of dye per g of particles for the hollow spheres hydrothermally treated at 140 °C (Figure 7a). The trend of dye adsorption tracks the trend in surface areas of the hollow spheres prepared at different hydrothermal treatment temperatures (Table 1), with the quantity of dye adsorbed decreasing with surface area. It should also be noted that although the photodegradation curves in Figure 7a may appear to be merely a continuance of dye adsorption without photodegradation, a similar test was performed with a significantly longer dark adsorption period of 24 h prior to UV light illumination, which showed similar dye adsorption capacity, confirming that adsorption desorption equilibrium had been reached within only 30 min. This strong dye adsorption may be in part due to the presence of the residual silica in the particle shell, which would be expected to show preferential affinity for positively charged adsorbents.[48,50] Indeed, the residual silica may be beneficial for the photocatalysis of the spheres by improving their colloidal stability through increased surface charging (the isoelectric point of silica is at a lower pH than TiO_2), or due to favorable modification of the bandgap of TiO_2, as has been observed previously.[46,50,51]

As a control, nonhollow hydrothermally treated SiO_2@TiO_2 particles (treated at pH 7 to prevent dissolution of the SiO_2 core, and at 2 mg mL^{-1} SiO_2, 140 °C, 6 h) were subjected to the same photocatalytic test. As can be observed in Figure 7a,

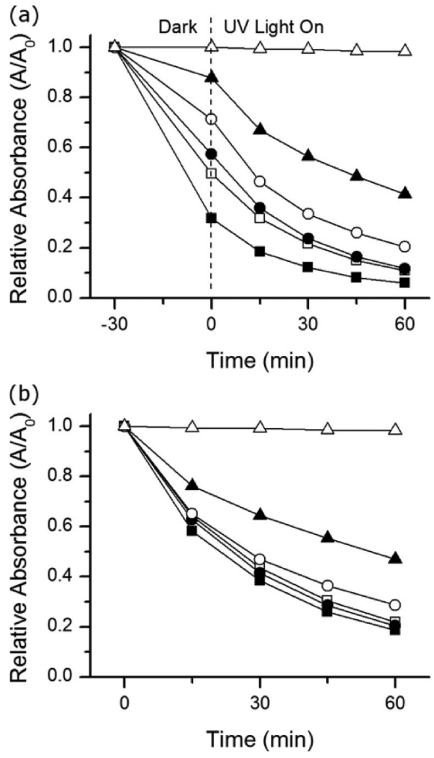

Figure 7. Photocatalytic methylene blue (MetB) UV decolouration test results, (a) showing the dark adsorption of the dye, and (b) with curves normalized to each sample's respective concentration of free MetB at the 0 min time point in a. Curves correspond to the hollow spheres hydrothermally synthesized (pH 12, 2 mg mL^{-1} SiO_2, 6 h) at 140 °C (■), 180 °C (□), 220 °C (●), and 140 °C followed by 500 °C calcination and base etching (▲), nonhollow SiO_2@TiO_2 particles hydrothermally treated at 140 °C (pH 7, 2 mg mL^{-1} SiO_2, 6 h) (○), and MetB in the absence of added TiO_2 (Δ).

dx.doi.org/10.1021/am3016922 | ACS Appl. Mater. Interfaces 2012, 4, 6062−6070

the adsorption capacity of these particles was substantially less than the corresponding hollow spheres synthesized at 140 °C. The increased adsorption capacity of the hollow spheres relative to these SiO_2@TiO_2 spheres may be due to the hollow geometry, possibly increasing the accessible surface area of the particles, or also perhaps due to the residual silica present in the TiO_2 shell, which would be absent in the SiO_2@TiO_2 particles, where the available silica would be confined to the core of the particles.

When the photocatalytic degradation curves were normalized to the concentration of dye present in solution after dark adsorption (i.e., at time point 0, when the UV light was turned on), the photocatalytic efficiency of the three hydrothermally treated samples prepared at 140 °C, 180 and 220 °C were observed to be quite comparable (Figure 7b), with pseudo-first-order rate constants varying by ≤10% in the range of 4.4−4.9 × 10^{-4} s^{-1}. Thus the trade-off between surface area and crystallinity appears to hold the net photocatalytic activity of the hollow spheres approximately constant with change in the hydrothermal treatment temperature; the crystallinity of the hollow spheres increases with treatment temperature, thus compensating for any decline in photocatalytic activity of the spheres due to loss in surface area. As the hollow spheres prepared at 140 °C have a similar rate constant as those prepared at higher temperature, the higher adsorption capacity of these particles renders 140 °C to be the optimal hydrothermal synthesis temperature to produce spheres for use in photocatalytic applications. This low hydrothermal temperature optimum is also advantageous from an economic and environmental perspective, as the 140 °C spheres required the least energy to be synthesized, and 140 °C is a very mild synthesis temperature compared to typical TiO_2 processing conditions.

With a loss in surface area without concomitant increase in crystallinity, the 140 °C hydrothermally treated hollow spheres which were subsequently calcined and base etched would be expected to exhibit a decline in photocatalytic activity relative to the uncalcined hollow spheres. This is indeed the case, as calcination and removal of residual silica led to not only a significant decline in the dye adsorption capacity of this sample (Figure 7a), but also a substantial decline in the pseudofirst order rate constant to 2.2 × 10^{-4} s^{-1} (Figure 7b). This decline in adsorption capacity of the calcined spheres, despite possessing a similar surface area as the 220 °C hydrothermally treated sample (Table 1), would seem to confirm the role of residual silica in enhancing dye adsorption. Similarly, interparticle sintering and aggregation during calcination, and possibly the presence of residual sodium from the NaOH etch (see the Supporting Information Table 1), may have adversely affected the colloidal stability of the calcined hollow spheres, impacting their photocatalytic performance.

3. CONCLUSION

In this study, we prepared mesoporous anatase TiO_2 hollow spheres with exceptional surface areas and photocatalytic activity by the controlled hydrothermal etching of silica templates. Because of these properties, we anticipate that these robust, nonfracturing hollow spheres will be advantageous to use in a variety of applications. The mild hydrothermal processing conditions employed by this synthesis method, and the simple "one pot" nature of the process wherein the silica template is etched while simultaneously crystallizing a mesoporous TiO_2 shell, without use of templating surfactants, as well as the fast silica etching achieved, should all significantly aid in the practical manufacturability of these particles at scale over elaborate hierarchical nanomaterials synthesized by more complex and expensive means. Similarly, the use of nontoxic aqueous reaction conditions and low energy input renders this process an environmentally friendly "green" synthesis approach to achieve templated mesoporous functional materials. All of these synthesis features are important for the translation of advanced materials from the laboratory to industry.

4. EXPERIMENTAL SECTION

4.1. Materials. Tetraethyl orthosilicate (TEOS) (99%, Sigma) and titanium(IV) butoxide (TBOT) (97%, Sigma) were purchased as precursors for each reaction step and used without further purification. Ammonium hydroxide (28% solution, Sigma), ethanol (EtOH) (99%, ACS reagent grade), methylene blue (MetB) (>96%, Sigma), and hydroxypropyl cellulose (HPC) (100,000 MW, Sigma) were purchased and used without further purification.

4.2. Silica Core Synthesis. Silica cores used as templates were synthesized according to the Stöber method.[33] Briefly, TEOS was added to a solution of NH_4OH in EtOH under vigorous stirring, such that the final concentrations of reagents were approximately 3.33 M H_2O, 1.4 M NH_4OH, and 0.2 M TEOS. The flask was sealed and allowed to stir vigorously for at least 10 h overnight before recovering the particles by centrifugation and washing thrice with EtOH. After washing, the sample was dried at 70 °C in air.

4.3. TiO_2 Coating of Silica Cores. The silica cores as synthesized previously were coated with TiO_2 via a colloidal sol−gel deposition reaction similar to that proposed by Lee et al.[35] Dried silica particles were dispersed into EtOH by sonication (Branson, 160 W) and then deionized water and HPC were added, and the solution was stirred to dissolve the HPC. A 40% v/v solution of TBOT in EtOH was then added to the first solution under agitation dropwise over the course of 1 h with a syringe pump, such that the final concentrations of reagents in the solution were 0.45 M H_2O, 3 mg mL^{-1} HPC, and 0.12 M TBOT. Once infusion of the TBOT solution was complete, the mixture was heated to 85 °C and stirred for 1.5 h. After cooling, the product was washed thrice with EtOH via centrifugation, and then dispersed into deionized water at a known SiO_2 concentration for subsequent hydrothermal treatments.

4.4. Hydrothermal Treatment. Hydrothermal treatment of the SiO_2@TiO_2 particles was performed in a PTFE-lined stainless steel pressure vessel (Parr). Aqueous SiO_2@TiO_2 particle suspension with a known silica concentration was mixed with deionized water, NaOH, and HCl to adjust the silica concentration and pH. The vessels (~66% fill fraction) were then placed in a furnace to heat to temperature at a rate of 2 °C min^{-1}, and held at temperature for a specified time before cooling. The particles were recovered and washed thoroughly with deionized water by centrifugation and dried at 70 °C in air before further use. The well-formed hollow spheres were robust and did not fracture or disintegrate from centrifugation or sonication.

4.5. Calcination and Base Etching. Some of the hydrothermally treated samples, after drying, were subsequently calcined in air at 500 °C for 2 h (Thermo, 1 °C min^{-1} ramp rate). After calcination, the samples were dispersed in 0.5 M NaOH solution at a concentration of 7.5 mg mL^{-1} by sonication, and then stirred at 50 °C in a sealed vessel for 24 h. The particles were washed thoroughly with deionized water by centrifugation and dried at 70 °C in air before further use.

4.6. Photocatalytic Tests. Particles were suspended into deionized water by sonication (10 min, 100 W, pulsed, Branson) at a concentration of 1 mg mL^{-1}. This particle suspension was then added to an aqueous MetB stock solution in a 250 mL PTFE beaker such that the final concentrations of particles and MetB were 0.05 mg mL^{-1} and 5 mg L^{-1}, respectively, and the total solution volume was 125 mL. This solution was mixed well and stored in the dark for 30 min to achieve adsorption−desorption equilibrium. The beaker was then placed under a UVC light source (UVP CL-1000 254 nm, ~6.67 mW cm^{-2}) and 1 mL aliquots were withdrawn at regular intervals and

stored in the dark. After the completion of the test, these aliquots were centrifuged at 15,000 rpm for 10 min to remove suspended particles, and the concentration of MetB was determined by measuring the absorbance of the supernatant at 668 nm with a spectrophotometer (BioTek Epoch). A 5 mg L^{-1} MetB solution without added particles was subjected to the same test, as a control.

4.7. Characterization. The size and surface morphology of the particles were analyzed with a transmission electron microscope (TEM, Philips CM-10, 60 keV). The crystallinity of the prepared samples was assessed through X-ray diffraction (XRD, Bruker D8 Focus, 1.54 Å Cu Kα radiation) analysis. The surface area of the materials (predried at 300 °C in N_2) was calculated from the Brunauer–Emmett–Teller (BET) equation with data from N_2 adsorption isotherms obtained at 77 K (Micrometrics Gemini VII 2390 Surface Area Analyzer). The presence of residual silica was detected through use of Fourier-transform infrared spectroscopy (FTIR, Bruker Tensor 27) of powdered samples in KBr pellets. The elemental compositions of the samples were determined from a standardless ZAF fit of energy dispersive X-ray spectra (EDX, Zeiss LEO Gemini 1530, 15 kV, EDAX Genesis).

■ ASSOCIATED CONTENT

Supporting Information

TEM, SEM, and EDX data. This material is available free of charge via the Internet at http://pubs.acs.org.

■ AUTHOR INFORMATION

Corresponding Author

*Address: Department of Chemical Engineering, 200 University Avenue W, Waterloo, ON N2L3G1, Canada. Tel: (519) 888-4567, ext. 38605. Fax: (519) 888-4347. E-mail: frank.gu@uwaterloo.ca.

Author Contributions

†These authors contributed equally. The manuscript was written through contributions of all authors. All authors have given approval to the final version of the manuscript.

Notes

The authors declare no competing financial interest.

■ ACKNOWLEDGMENTS

This work is financially supported by Natural Sciences and Engineering Research Council of Canada.

■ ABBREVIATIONS

EtOH, ethanol; TEOS, tetraethyl orthosilicate; TBOT, titanium(IV) butoxide; MetB, methylene blue; HPC, hydroxypropyl cellulose

■ REFERENCES

(1) Liu, G.; Wang, L.; Yang, H. G.; Cheng, H.; Lu, G. Q. *J. Mater. Chem.* **2010**, *20*, 831–843.
(2) Chen, X.; Liu, L.; Yu, P. Y.; Mao, S. S. *Science* **2011**, *331*, 746–750.
(3) Henderson, M. A. *Surf. Sci. Rep.* **2011**, *66*, 185–297.
(4) Weir, A.; Westerhoff, P.; Fabricius, L.; Hristovski, K.; von Goetz, N. *Environ. Sci. Technol.* **2012**, *46*, 2242–2250.
(5) Yella, A.; Lee, H.; Tsao, H. N.; Yi, C.; Chandiran, A. K.; Nazeeruddin, M. K.; Diau, E. W.; Yeh, C.; Zakeeruddin, S. M.; Graetzel, M. *Science* **2011**, *334*, 629–634.
(6) Chong, M. N.; Jin, B.; Chow, C. W. K.; Saint, C. *Water Res.* **2010**, *44*, 2997–3027.
(7) Daskalaki, V. M.; Frontistis, Z.; Mantzavinos, D.; Katsaounis, A. *Catal. Today* **2011**, *161*, 110–114.
(8) Sturini, M.; Speltini, A.; Maraschi, F.; Profumo, A.; Pretali, L.; Irastorza, E. A.; Fasani, E.; Albini, A. *Appl. Catal., B* **2012**, *119*, 32–39.
(9) Ismail, A. A.; Bahnemann, D. W. *J. Mater. Chem.* **2011**, *21*, 11686–11707.
(10) Chen, D.; Cao, L.; Huang, F.; Imperia, P.; Cheng, Y.; Caruso, R. A. *J. Am. Chem. Soc.* **2010**, *132*, 4438–4444.
(11) Li, S.; Shen, Q.; Zong, J.; Yang, H. *J. Alloys Compd.* **2010**, *508*, 99–105.
(12) Roy, P.; Berger, S.; Schmuki, P. *Angew. Chem., Int. Ed.* **2011**, *50*, 2904–2939.
(13) Hu, J.; Chen, M.; Fang, X.; Wu, L. *Chem. Soc. Rev.* **2011**, *40*, 5472–5491.
(14) Liu, J.; Qiao, S. Z.; Chen, J. S.; Lou, X. W.; Xing, X.; Lu, G. Q. *Chem. Commun.* **2011**, *47*, 12578–12591.
(15) Feng, X.; Yang, L.; Liu, Y. *Appl. Surf. Sci.* **2010**, *257*, 756–761.
(16) Yu, J.; Liu, W.; Yu, H. *Cryst. Growth Des.* **2008**, *8*, 930–934.
(17) Liu, Z.; Bai, H.; Sun, D. *Appl. Catal. B* **2011**, *104*, 234–238.
(18) Jiao, Y.; Peng, C.; Guo, F.; Bao, Z.; Yang, J.; Schmidt-Mende, L.; Dunbar, R.; Qin, Y.; Deng, Z. *J. Phys. Chem. C* **2011**, *115*, 6405–6409.
(19) Ding, S.; Chen, J. S.; Wang, Z.; Cheah, Y. L.; Madhavi, S.; Hu, X.; Lou, X. W. *J. Mater. Chem.* **2011**, *21*, 1677–1680.
(20) Lai, X.; Li, J.; Korgel, B. A.; Dong, Z.; Li, Z.; Su, F.; Du, J.; Wang, D. *Angew. Chem., Int. Ed.* **2011**, *50*, 2738–2741.
(21) Dadgostar, S.; Tajabadi, F.; Taghavinia, N. *ACS Appl. Mater. Interfaces* **2012**, *4*, 2964–2968.
(22) Yu, J.; Li, Q.; Shu, Z. *Electrochim. Acta* **2011**, *56*, 6293–6298.
(23) Yao, Y.; Yao, J.; Narasimhan, V. K.; Ruan, Z.; Xie, C.; Fan, S.; Cui, Y. *Nat. Commun.* **2012**, *3*, 664.
(24) Wu, X.; Lu, G. Q.; Wang, L. *Energy Environ. Sci.* **2011**, *4*, 3565–3572.
(25) Zhang, Q.; Li, W.; Liu, S. *Powder Technol* **2011**, *212*, 145–150.
(26) Kim, C.; Kim, S.; Oh, W.; Choi, M.; Jang, J. *Chem.—Eur. J.* **2012**, *18*, 4902–4908.
(27) Nelson, K.; Deng, Y. *Langmuir* **2008**, *24*, 975–982.
(28) Ding, S.; Chen, J. S.; Qi, G.; Duan, X.; Wang, Z.; Giannelis, E. P.; Archer, L. A.; Lou, X. W. *J. Am. Chem. Soc.* **2011**, *133*, 21–23.
(29) Peng, T.; Zhao, D.; Dai, K.; Shi, W.; Hirao, K. *J Phys Chem B* **2005**, *109*, 4947–4952.
(30) Tian, G.; Fu, H.; Jing, L.; Xin, B.; Pan, K. *J. Phys. Chem. C* **2008**, *112*, 3083–3089.
(31) Yu, J.; Su, Y.; Cheng, B.; Zhou, M. *J. Mol. Catal. A: Chem.* **2006**, *258*, 104–112.
(32) Yu, J.; Wang, G.; Cheng, B.; Zhou, M. *Appl. Catal., B* **2007**, *69*, 171–180.
(33) Stober, W.; Fink, A.; Bohn, E. *J. Colloid Interface Sci.* **1968**, *26*, 62–&.
(34) Bogush, G.; Tracy, M.; Zukoski, C. *J. Non Cryst. Solids* **1988**, *104*, 95–106.
(35) Lee, J.; Kong, S.; Kim, W.; Kim, J. *Mater. Chem. Phys.* **2007**, *106*, 39–44.
(36) Joo, J. B.; Zhang, Q.; Lee, I.; Dahl, M.; Zaera, F.; Yin, Y. *Adv. Funct. Mater.* **2012**, *22*, 166–174.
(37) Brinker, C. *J. Non Cryst. Solids* **1988**, *100*, 31–50.
(38) Yanagisawa, K.; Yamamoto, Y.; Feng, Q.; Yamasaki, N. *J. Mater. Res.* **1998**, *13*, 825–829.
(39) Pan, J. H.; Cai, Z.; Yu, Y.; Zhao, X. S. *J. Mater. Chem.* **2011**, *21*, 11430–11438.
(40) Wu, M.; Lin, G.; Chen, D.; Wang, G.; He, D.; Feng, S.; Xu, R. *Chem. Mater.* **2002**, *14*, 1974–1980.
(41) Yu, Q.; Wang, P.; Hu, S.; Hui, J.; Zhuang, J.; Wang, X. *Langmuir* **2011**, *27*, 7185–7191.
(42) Yoon, S. B.; Woo, B.; Chung, S. J.; Yun, W. S. *J. Nanosci. Nanotechnol.* **2012**, *12*, 1604–1607.
(43) Alivisatos, A. *J. Phys. Chem.* **1996**, *100*, 13226–13239.
(44) Goldstein, A.; Echer, C.; Alivisatos, A. *Science* **1992**, *256*, 1425–1427.
(45) Pasquarello, A.; Car, R. *Phys. Rev. Lett.* **1997**, *79*, 1766–1769.
(46) Gao, X.; Wachs, I. *Catal. Today* **1999**, *51*, 233–254.
(47) Liu, J.; Li, M.; Wang, J.; Song, Y.; Jiang, L.; Murakami, T.; Fujishima, A. *Environ. Sci. Technol.* **2009**, *43*, 9425–9431.

(48) Zhang, M.; Shi, L.; Yuan, S.; Zhao, Y.; Fang, J. *J. Colloid Interface Sci.* **2009**, *330*, 113−118.
(49) Yang, P.; Zhao, D.; Margolese, D.; Chmelka, B.; Stucky, G. *Nature* **1998**, *396*, 152−155.
(50) Jafry, H. R.; Liga, M. V.; Li, Q.; Barron, A. R. *Environ. Sci. Technol.* **2011**, *45*, 1563−1568.
(51) Fujishima, M.; Takatori, H.; Tada, H. *J. Colloid Interface Sci.* **2011**, *361*, 628−631.